International Forum on Aeroelasticity and Structural Dynamics
IFASD 2017
25-28 June 2017 Como, Italy

# DESIGN OF AN INNOVATIVE WING TIP DEVICE

**F. Toffol[1], F. Fonte[1], S. Ricci[1]**

[1]Dipartiment of Aerospace Science and Technology
Politecnico of Milano
via La Masa, 34 Milano 20156 Italy
francesco.toffol@polimi.it
federico.fonte@polimi.it
sergio.ricci@polimi.it

**Keywords:** wingtip devices, load control and alleviation.

**Abstract:** This paper describes the design of an active wing tip for a regional transport aircraft is presented. The device is designed with the double purpose of increase the aircraft efficiency and to alleviate gust loads by means of an actively controlled control surface included in it. The control system used for the actuation uses a Static Output Feedback (SOF) architecture, and it is computed by optimizing a quadratic norm ($H_2$) of the closed loop system.

## 1 INTRODUCTION

This document is devoted to the design and the implementation of Load Control and Alleviation (LC&A) technologies having the double target of increasing the aircraft efficiency, so reducing the fuel burn together with reducing the peak loads due to gust. These targets are pursued by using in a synergic way the conventional control surfaces (ailerons, flaps and elevator) together with new, dedicated control surfaces like the morphing leading edge and winglets. Concerning the Gust Load Alleviation (GLA) purpose, the benefits introduced by an innovative wingtip are investigated in terms of gust load alleviation capability and aerodynamic performances improvement.
Traditionally, the studies related to the shape of the tip of the wing are strongly motivated by the need to decrease the environmental impact as well as the direct costs due to the soaring fuel price and aim at reducing the lift induced drag, which during cruise conditions constitutes approximately 40% of the total drag.
A series of different and exotic wing tip devices have been proposed and this research field is very active, with several projects funded by the aerospace industry in the past few years [1–3]. The most successful solution is undoubtedly winglets, first introduced by Whitcomb [4] in the 1970s. This concept delivers benefits such as reduction in emissions and fuel consumption, directly translating into money savings for airlines, improvement of take-off and landing performances, with reduced community noise and payload or range increase.
On the other hand, adding winglets on small aircraft would not allow more airplanes to be parked at existing airport gates; often small aircraft are parked next to larger ones, with wings overlapping: the addition of winglets would aggravate the gate problem more than span extension.
A problem common to the wingtip devices is the potential increase in structural mass due to higher bending moments, which would frustrate the aerodynamic benefit.

Tackling the aforementioned issues, an innovative wingtip is designed as an alternative option to a traditional winglet: it is equipped with a dedicated control surface, which aims reducing the gust load through an active controller. This device can be used as a load control device during cruise and maneuver, optimizing the lift distribution span wise and reducing the additional wing root bending moment (WRBM) due to the wing span extension.
The design process can be summarized by the following steps:

- Geometrical sensitivity analysis aimed to find the most efficient solution for the load alleviation purpose.
- Aerodynamic performance evaluation with medium-fidelity tool.
- Structural layout identification and stress analysis.
- Preliminary configuration of a possible actuation system for the control surface.

## 2 GEOMETRY IDENTIFICATION

As pointed out in the introduction, a limiting factor for the wingtip devices (WTIP) is their extension; in this case study the allowable span increase for a typical 90 pax regional aircraft here considered is 10%.
A parametric study of possible solutions has been performed, investigating the effects of several parameters on the aero-structural response of the system.
Two possible configurations are here considered (Fig. 1): a wing tip with a movable trailing edge (Fig. 1(a)) and an all-movable surface (Fig. 1(b)).
The geometrical parameters used for the sensitivity analysis are illustrated in Fig. 2 and described in Tab. 1.
The evaluation of the performances and the tools used are described in the next sections.

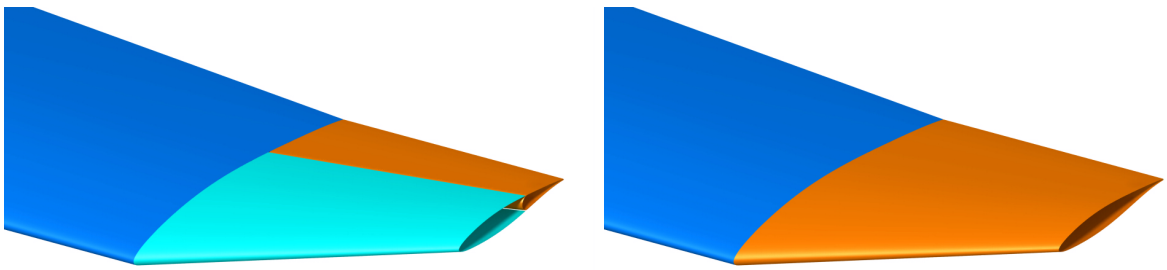

(a) Movable Trailing Edge (b) All-movable

Figure 1: Possible configuration considered

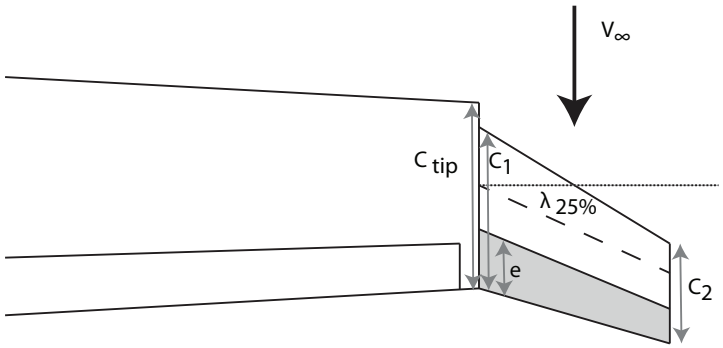


Figure 2: Design variables

| Inboard chord ratio | Taper ration | Flap hinge location | Sweep angle | Span | Diehdral |
|---|---|---|---|---|---|
| $\frac{C_1}{C_{tip}}$ | $\frac{C_2}{C_1}$ | $\frac{e}{C_1}$ | $\Lambda$ | L | $\Gamma$ |

Table 1: Design variables

### 2.1 The Aeroelastic Analysis Framework

The performances of the different WTIP configurations must be evaluated: for this reason a finite element method (FEM) model has been realized: it is representative of the reference aircraft and it is made by bar elements and concentrated masses; the aerodynamics is modeled with a doublet-lattice method (DLM). Fig. 3(a) shows the CAD representation of the reference aircraft, while Fig. 3(b) shows the aeroelastic stick model of the same airplane and used for the simulation.

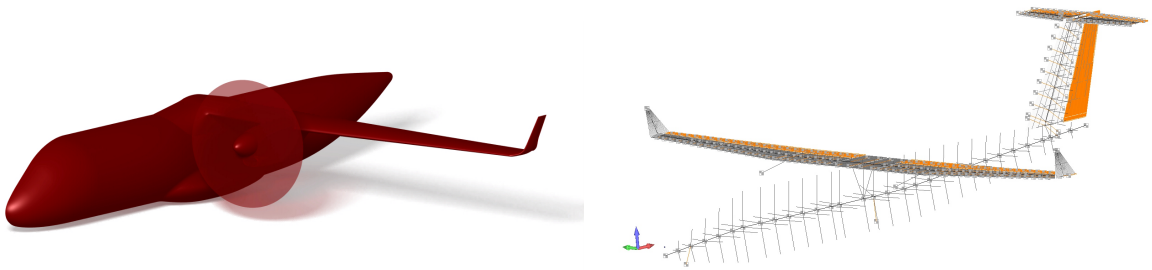

(a) Reference aircraft CAD model

(b) Reference aircraft stick model

Figure 3: Reference aircraft

The Aeroelastic Analysis Framework (AAF) is a Matlab-based procedure combining three modules:

- Wingtip parameterization module: this block creates the matrices of the aeroelastic problem, evaluating the structural properties and the aerodynamic forces due to structural motion, gust and command input.
- Aeroelastic Response Module (NeoRESP): this is the core of the analysis procedure. It solves the aeroelastic problem in frequency domain, providing several outputs.
- Result Assessment Module: the results of the analyses are collected and elaborated in order to obtain the desired quantity for the evaluation of the wingtip performances, which are mapped in 2D and 3D plots.

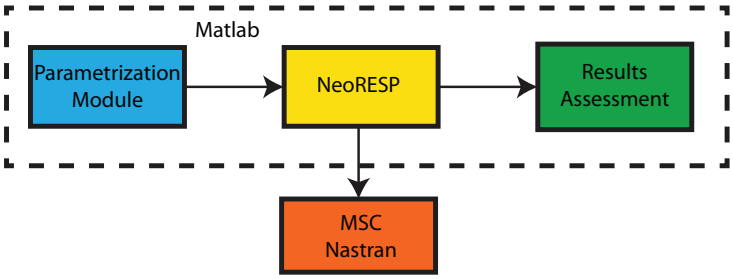


Figure 4: Aeroelastic Analysis Framework

NeoRESP is one of the module of NeoCASS [5]; it is based on a second order frequency domain formulation ad solves the dynamic response to gust (shaped according to CS 25 regulation) and command input.
Inputs are translated in frequency domain, the response is evaluated over the frequency of interest and then inverse-transformed to the time domain.
The AAF is used to investigate the aeroelastic response of the system to gust and command input; the most time-consuming procedure is the creation of the aerodynamic matrices through the parameterization module, hence them are assembled and stored in a database. This step is done only one time, speeding up the response analysis procedure: once collected, the same matrices can be used for several analyses without assembling the problem each time.
Using the AAF, a large population of WTIP has been produced; the simulation produced several output, such as nodal displacements, internal forces in bar elements, hinge moment of the control surface. Due to the different nature of the values obtained, a common methodology for the WTIP performance evaluation is mandatory.

### 2.2 Evaluation criteria for the AAF

To asses and compare the results obtained with NeoRESP, it is mandatory to establish an evaluation criteria that highlights the strength and the weakness of each configuration. The metric adopted consists in evaluating the open loop admittance between the input and the wing loads.
The transfer function (TF) from the input (gust or surface deflection) to the output (loads, hinge moment) is extracted from the assembled aeroelastic problem:

$$Z(j\omega) = H(j\omega)\delta_{wtip}(j\omega) \tag{1}$$

The transfer function obtained is evaluated at $\omega = 0$ providing its steady value $H(0)$; the dynamic performance is obtained evaluating a quadratic norm of the TF over a finite frequency range:

$$||H(j\omega)||_2 = \left[\int_{\omega_1}^{\omega_2} |H(j\omega)|^2 d\omega\right]^{\frac{1}{2}} \tag{2}$$

The frequency range used for the computation of the norm is 0–10 Hz, compatible with the bandwidth of the actuator used in a similar project [6–8].
The analyses have been performed in a cruise condition at an altitude of 6096m and a Mach of 0.52, which is the cruise condition of the reference aircraft.

### 2.3 Results of the AAF

The large amount of data obtained from the aforementioned AAF procedure are compared mapping the response obtained for different WTIP configuration; the relevant design parameter used are:

- $\frac{C_1}{C_{tip}}$: from 0.5 to 1, step 0.25.
- $\frac{C_2}{C_1}$: from 0.2 to 0.5, step 0.1.
- $\frac{e}{C_1}$: from 0.1 to 0.9, step 0.1.
- $\Lambda_{25\%C}$: from -20° to 40°, step 10°.
- L: from 0.5 to 1.5m, step 0.1m.
- $\Gamma$: from -25° to 85°, step 5°.

The responses indexes used for the evaluation of the WTIP aeroelastic performances are:

- The wing root bending moment (WRBM).
- The wing root torsional moment (WRTM).
- The ratio from WRBM to the hinge moment, which is an indicator of the cost to produce a change in the WRBM.
- The hinge moment (HM) of the control surface.

Both the flapped (blue) and all-movable(red) configuration have been analyzed; the results of the sensitivity analysis on the hinge axis location and span extension are presented as 3D maps in Fig. 5.

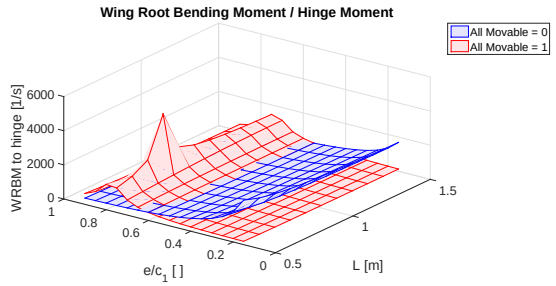


(a) $\frac{WRBM}{HM}$ vs. $\frac{e}{C_1}$ and span, sensitivity map

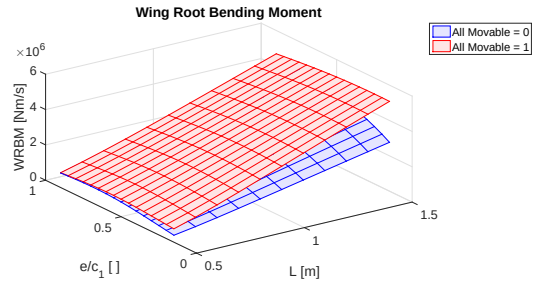


(b) WRBM vs. $\frac{e}{C_1}$ and span, sensitivity map

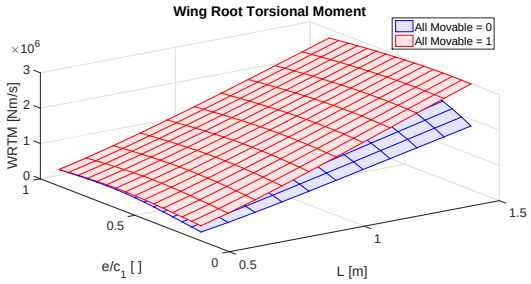


(c) WRTM vs. $\frac{e}{C_1}$ and span, sensitivity map

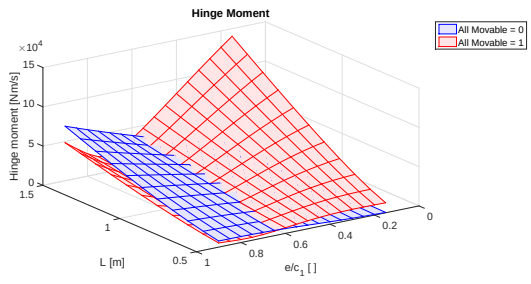


(d) HM vs. $\frac{e}{C_1}$ and span, sensitivity map

Figure 5: Loads sensitivity maps

The influence of the flapped configuration on WRBM and WRTM rises steeply changing the $\frac{e}{C_1}$ from 0.1 to 0.4 (Figs. 5(b) and 5(c)), while smaller variations are obtained for larger value; looking at the HM (Fig. 5(d)), it reaches larger value for the all-movable configuration.
Fig. 5(a) shows a region where the all-movable presents a peak: it is reached when the hinge axis in close to the 25%, hence the aerodynamic moment is low as shown in Fig. 5(d). In this condition the all-movable configuration is very effective from the actuation point of view because the torque required to the actuator are low, but it is near to the neutral static stability, which could generate instability phenomena, both static and dynamic.

Further investigation has been performed changing the sweep angle, producing sensitivity maps similar to the ones in Fig. 5. Fig 6 shows the results of this analysis, mapping the responses obtained varying the hinge axis location and the sweep angle; the analysis has been performed for different span of the WTIP.

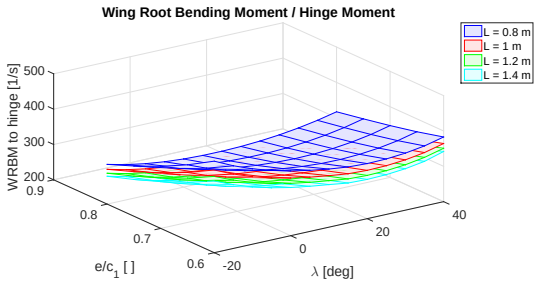


(a) $\frac{WRBM}{HM}$ vs. $\frac{e}{C_1}$ and sweep, sensitivity map

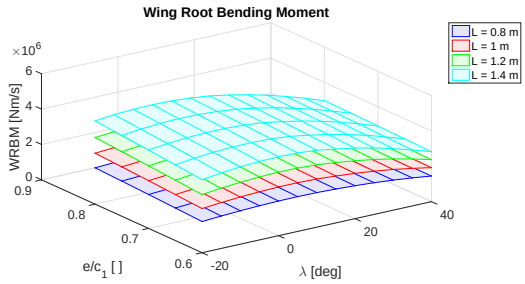


(b) WRBM vs. $\frac{e}{C_1}$ and sweep, sensitivity map

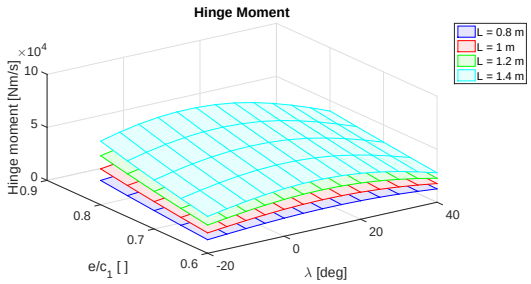


(c) HM vs. $\frac{e}{C_1}$ and sweep, sensitivity map

Figure 6: Loads sensitivity to sweep angle and hinge location

From results shown in Fig. 6 it is possible to say that sweep angle near $0°$ have produces the highest wing root bending moment and hinge moment, while WRBM/HM ratio is maximum for $\Lambda > 30°$or $< 0°$.
So far, static responses have been taken into account, hence the steady value of the transfer function $H(0)$; concerning the gust sensitivity and the surface effectiveness over the frequency range of interest, the norm shown in Eq. (2) must be used.
In this case the parameters that mostly affect the responses are the dihedral and the span extension, which directly influence the projected area of the wingtip.

In Fig. 7(a) the influence on WRBM of the dihedral angle is presented, both for all-movable and flapped surface. The upper plot shows three curves: the black one is the difference between the norm of the transfer function from gust angle to WRBM for a reference WTIP with $\Gamma = 85°$ and configurations with different angles $||H_{\Gamma=xx° \; WRBM,gust}||_2 - ||H_{\Gamma=85° \; WRBM,gust}||_2$; the blue/red curve is the difference, for flapped/all-movable configuration, between the norm of the transfer function from surface deflection to WRBM for a reference WTIP with $\Gamma = 85°$ and configurations with different angles $||H_{\Gamma=xx° \; WRBM,\delta WTIP}||_2 - ||H_{\Gamma=85° \; WRBM,\delta WTIP}||_2$. In the lower plot of Fig. 7(a) the blue/red curve is the difference between the blue/red cureve and the black one of the upper plots, values $0$ means that the sensitivity of the WRBM to the surface deflection is higher that the sensitivity to the gust angle.
In Fig. 7(b) the same same analysis is performed considering the span variation, the reference is a WTIP 1m width.

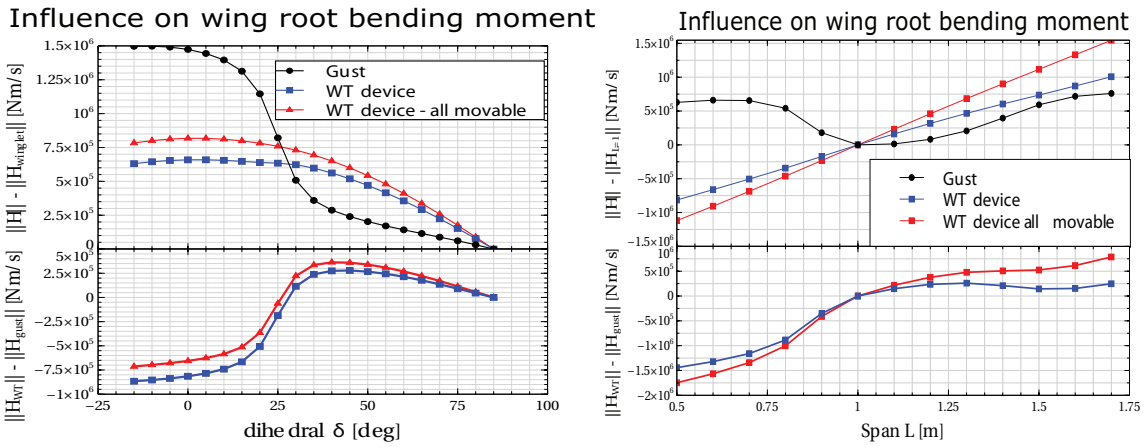


(a) WRBM norm sensitivity to dihedral

(b) WRBM norm sensitivity to span

Figure 7: Gust sensitivity maps for dihedral and span

On the basis of the results obtained, a reduced set of configurations has been extracted and it is reported in Tab. 2; on the basis of the consideration so far drawn, only ID1 and ID3 has been have been selectd for the closed loop analysis.

| ID | $\frac{C_1}{C_{tip}}$ | $\frac{C_2}{C_1}$ | $\frac{e}{C_1}$ | $\Lambda$ [deg] | L [m] | $\Gamma$ [deg] | All-Movable |
|---|---|---|---|---|---|---|---|
| 1 | 1 | 0.5 | 0.35 | 35 | 1.5 | 40 | no |
| 2 | 1 | 0.5 | 0.35 | -20 | 1.5 | 40 | no |
| 3 | 1 | 0.5 | 0.35 | 35 | 1 | 40 | no |
| 4 | 1 | 0.5 | 0.35 | 35 | 1.5 | 0 | yes |
| 5 | 1 | 0.5 | 0.7 | -20 | 1.5 | 40 | yes |
| 6 | 1 | 0.5 | 0.7 | 35 | 1.5 | 40 | yes |

Table 2: Best solutions obtained

From the most promising solutions above illustrated, the all-movable have been excluded: their implementation on the reference aircraft means changing the whole external wing structure and creating a single and stiff joint between the wing and the surface. Furthermore, the actuation system would result complex and without the possibility of redundancy.
The negative sweep angle solution is eliminated due to its negative influence on the aeroelastic behavior of the aircraft.

The remaining two configurations, ID1 e ID3, are used for the evaluation of the active controller; the closed loop analyses are performed using the SOF controller described in [9], this kind of analysis shows the effective GLA capabilities of the designed WTIP. The controller is based on the use of accelerometric measurements taken on the wing, as well as the rigid motion of the aircraft obtained from an Inertial Measurement Unit (IMU), the location of the sensors is shown in Fig. 8. The SOF controller requires the definition of a cost function, selecting the performances that will be the output of the closed loop transfer function whose $\mathcal{H}_2$ norm will be minimized. In Eq (3) J is the cost function, $\mathbf{z}$ are the performances an $\mathbf{u}$ are the inputs, which are a linear combination of the measurements: $\mathbf{u} = -\mathbf{G}\mathbf{y}$; $\mathbf{W_{zz}}$ and $\mathbf{W_{uu}}$ are weighting matrices.

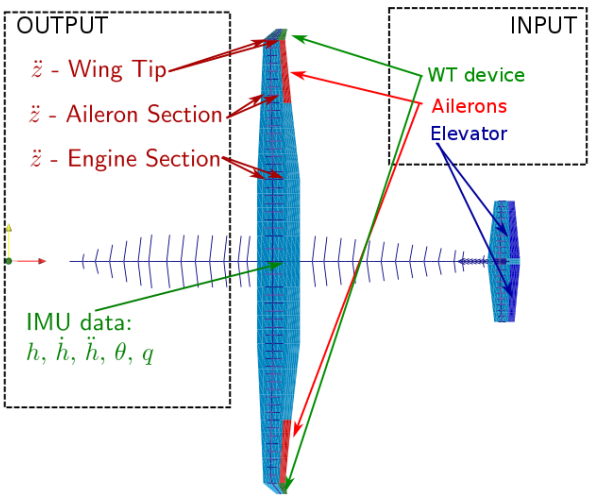


Figure 8: Measurements and control surfaces used by the GLA controller.

$$J = \frac{1}{2}\int_0^\infty [\mathbf{z}^\mathbf{T}\mathbf{W}_{\mathbf{zz}}\mathbf{z} + \mathbf{u}^\mathbf{T}\mathbf{W}_{\mathbf{uu}}\mathbf{u}] \tag{3}$$

The performances considered here are:

- bending moment at the wing root and the engine section;
- torsional moments at the wing root and engine section;
- pitch angle;
- pitch angular velocity;

The torsional and bending moments are the main targets of the GLA controller, the pitch angle and rate are included in the cost function with a small weight in order to ensure an adequate damping for the rigid motion of the aircraft. The evaluation of the closed loop transfer function requires also the definition of the disturbances, which are taken to be the gust input and the noise on the measurements, with a shaping filter used to define the frequency content of the gust in order to reproduce that of a deterministic 1-cos gust.

The best way to compare the results obtained is a bending/torsion envelope, where the load, obtained for different gust lengths, are added to the loads of the cruise condition.

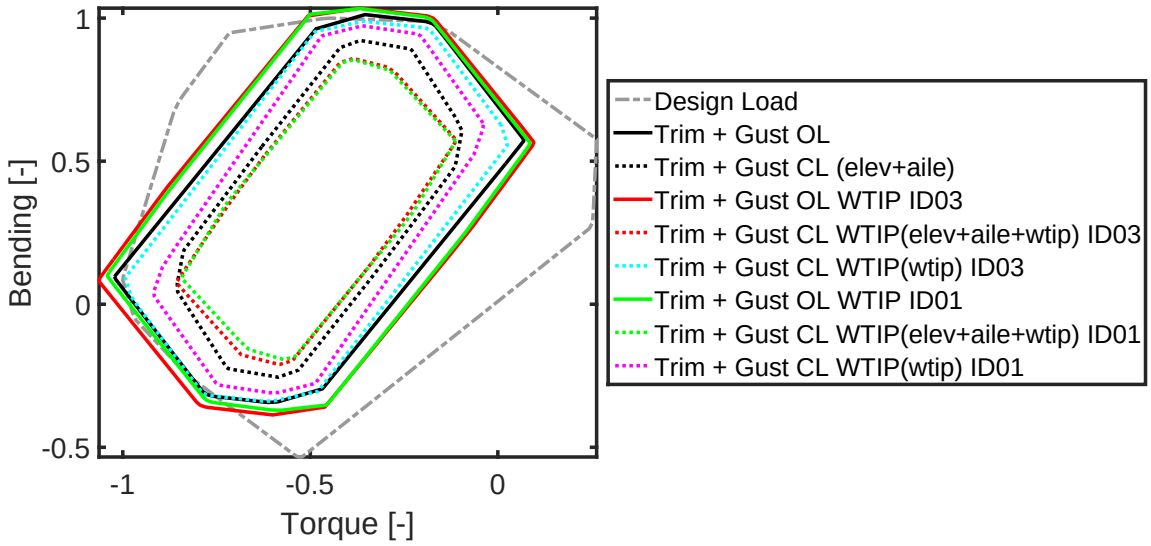


Figure 9: Adimensional Bending-Torsion envelope with SOF controller

Fig. 9 shows how the controlled aero-servo-elastic system wing root load envelope is completely include inside the design load envelope of the reference aircraft when the controller is turned on; some points of the open loop response fall outside the reference envelope because of the span extension, both for configuration 1 and 3.
The results in terms of alleviation capabilities are similar for the two solutions, but due to the lower hinge moments and to the lower deflection performed by the SOF controller, solution ID=3 is more suitable; in fact the lower required torques imply a smaller and lighter actuation system.

## 3 AERODYNAMIC PERFORMANCE EVALUATION

Once the best solution of the WTIP has been identified, an evaluation of the aerodynamic performances has been carried out; the deterioration of the efficiency of the aircraft is an undesired effect. For this reason a quasi-3D method has been adopted, which corrects the results of a panel method (Morino) with a RANS solver [10].
It is considered the rigid half-wing isolated, with symmetric boundary condition on the symmetry plane; the lift over drag ratio (LoD or efficiency) is evaluated at the lift necessary to counteract the weight, hence the analyses are performed at a fixed $C_L$.

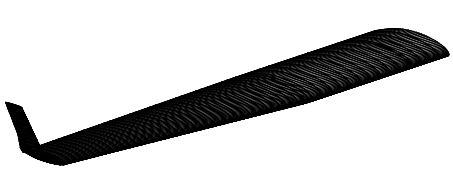

(a) Reference wing

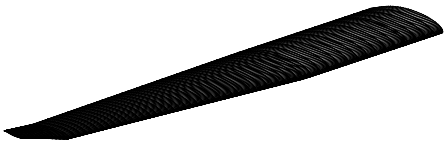

(b) Innovative wingtip

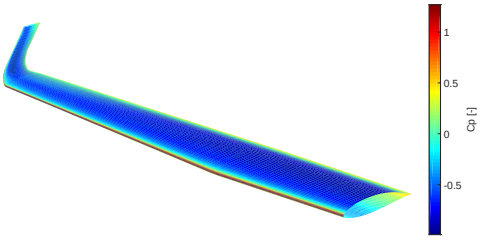


(c) Reference wing $C_P$ distribution in cruise

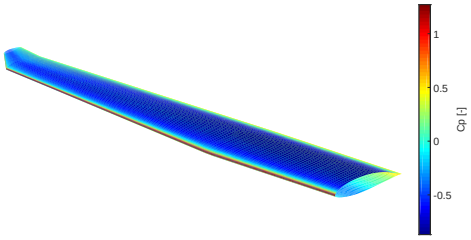


(d) Innovative wingtip $C_P$ distribution in cruise

Figure 10: Aerodynamic mesh and $C_P$ distribution in cruise for Morino's method

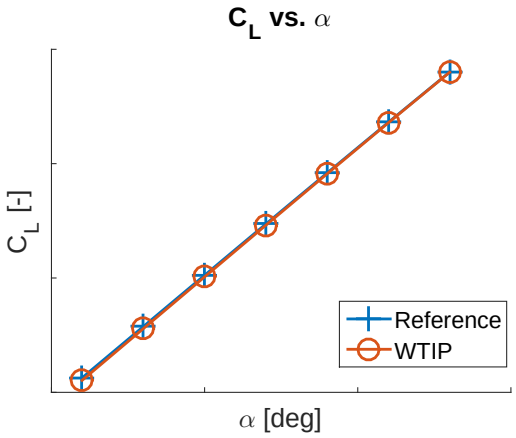


(a) $C_L$vs.$\alpha$

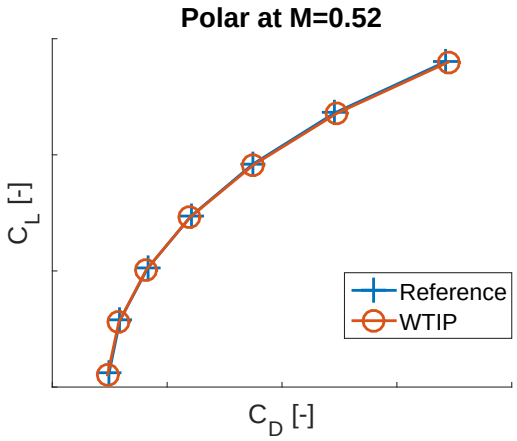


(b) Polar

Figure 11: Aerodynamic performances at M=0.52, quasi-3D method

The aerodynamic performances of the two wings are almost the same and the relevant results are reported in Tab. 3.

| Wing | $\alpha$ | $C_L$ | $C_D$ | E |
|---|---|---|---|---|
| Reference | -0.17° | 0.49 | 0.016195 | 30.41 |
| Innovative WTIP | -0.11° | 0.49 | 0.016105 | 30.58 |

Table 3: Aerodynamic performances in cruise condition

Despite of an higher angle of attack $\alpha$, the wing equipped with the innovative WTIP is more efficient that the reference one of about 0.56%.

Another important parameter that must be considered is the lift distribution span wise, in order to quantify the additional WRBM introduced by the span extension.
Looking at the aerodynamic component of the WRBM, it is decreased of 0.8% with the flapped surface fixed at 0°, it is possible to use this kind of surface to redistribute the aerodynamic load span wise, as Fig. 12 shows: an upward deflection of 5° reduces the aerodynamic WRBM of 3.4% while a downward one increases the load of 0.5% w.r.t. the reference wing.

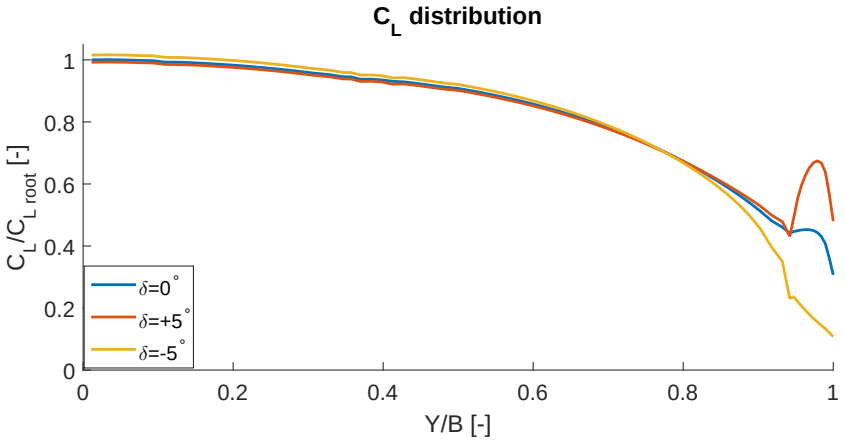


Figure 12: $C_L$ span wise distribution

## 4 STRESS ANALYSIS

Once assessed the GLA capabilities and the aerodynamic performances, the design of the internal structure is performed. The innovative wing tip is designed as a conventional aluminum wingbox, made of skins, stiffener, spar, ribs and spar cap.
A FEM model of the load carrying box has been realized in order to check the stress level inside the components. The model is integrated in the reference aircraft stick model and several trim cases and gusts have been simulated. The worst gust case is added to the relative trim case as prescribed by CS 25 regulation.
The areas mostly stressed are the connection with the movable surface; the maximum stress level experienced by the component is, following the Von Mises criteria ($\sigma_{VM}$), about 150 MPa, which is well below the yield limit of an aeronautic aluminium alloy, such as AL7075-T6, which is around 500MPa.

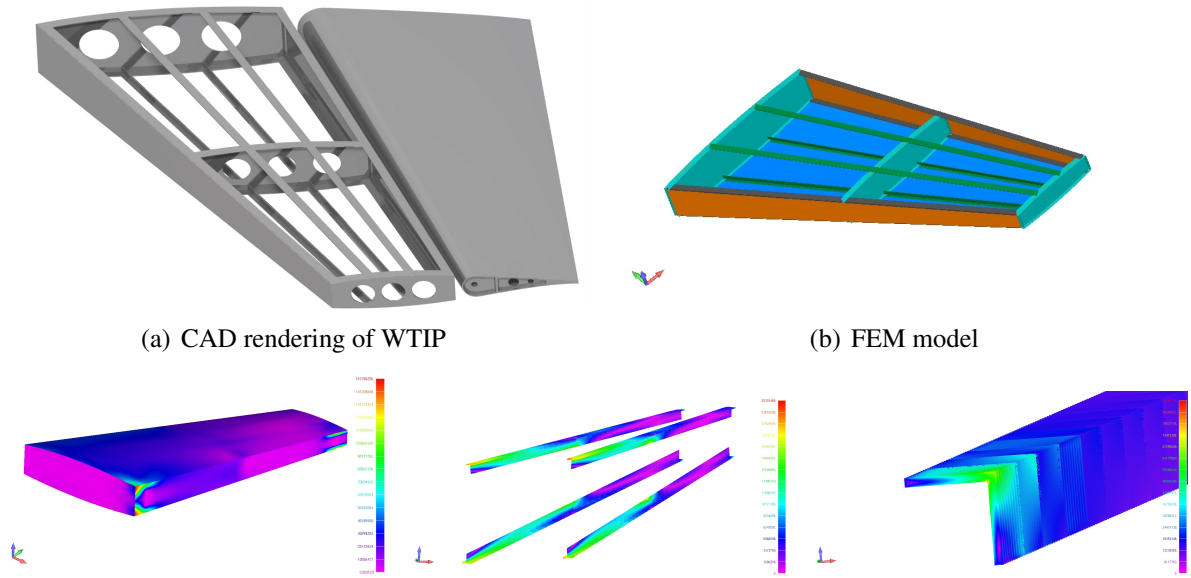

(a) CAD rendering of WTIP (b) FEM model

(c) Plate element $\sigma_{VM}$ (d) Stiffener cross section $\sigma_{VM}$ (e) Spar cap cross section $\sigma_{VM}$

Figure 13: FEM model and main stress analysis results

## 5 ACTUATION SYSTEM

One of the most critical system of the innovative wing tip device is the actuation system, which has to guarantee the deflection required by the controller, satisfying dynamic performance such as bandwidth. For this reason, an envelope of the limit condition in terms of static requirements (hinge moment during trim) and dynamic ones (deflection and torque vs. time) is presented in the following.

The deflection applied to the control surface is the one calculated by the SOF controller, a saturation limit on the deflection rate of $100°/s$ is imposed in order to avoid excessive rates during control, which could not been reached by a physical actuator.

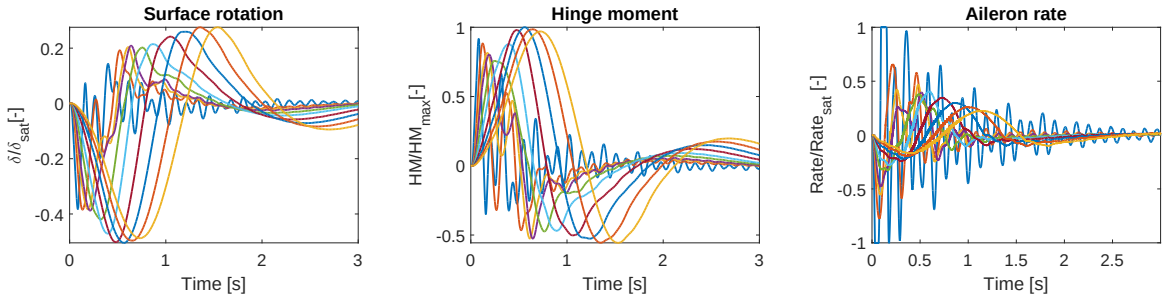


(a) Rotation required by SOF controller (b) Torque required by SOF controller (c) Rate required by SOF controller

Figure 14: Tim history: deflection and torque required by SOF controller

Fig. 15(b) highlights the rate saturation, in fact the envelope is cut with a vertical line in correspondence of the limit.

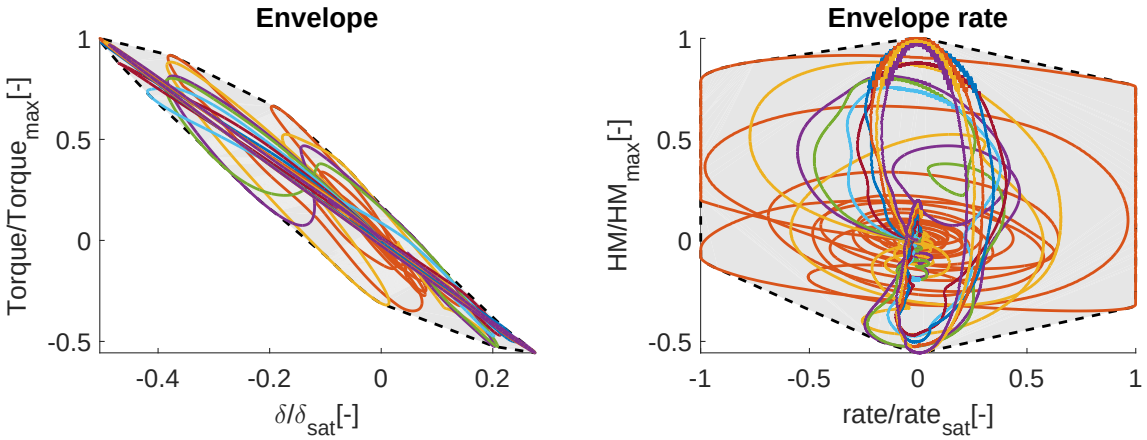


(a) Torque-rotation envelope

(b) Torque-rate envelope

Figure 15: Envelopes

Starting from the results above illustrated, an initial actuation layout is proposed: two Electro-Mechanical Actuator (EMA) are connected to the movable surface with a rod-crank mechanism, shown in Fig. 16(a). The relation between actuator force and hinge moment can be obtained from Fig. 16(b) and it is expressed in (4).

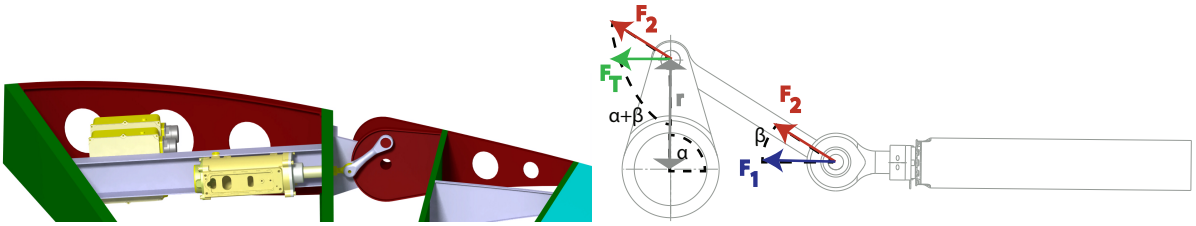


(a) Actuation layout

(b) Actuation forces

Figure 16: Drawing of the crank-rod mechanism

$$\begin{cases} F_2 = \frac{F_1}{\cos\beta} = \frac{F_{actuator}}{\cos\beta} \\ F_T = F_2 \sin(\alpha+\beta) \\ M = F_T r = \frac{F_{actuator}\sin(\alpha+\beta)}{\cos\beta} \end{cases} \tag{4}$$

Following the (4) it is possible to draw stroke-axial force and speed-axial force envelopes, obtaining the sizing values of the actuator. The results are influenced by the leverage of the kinematic; the aims of this analysis is the identification of the possible solution that could be implemented.

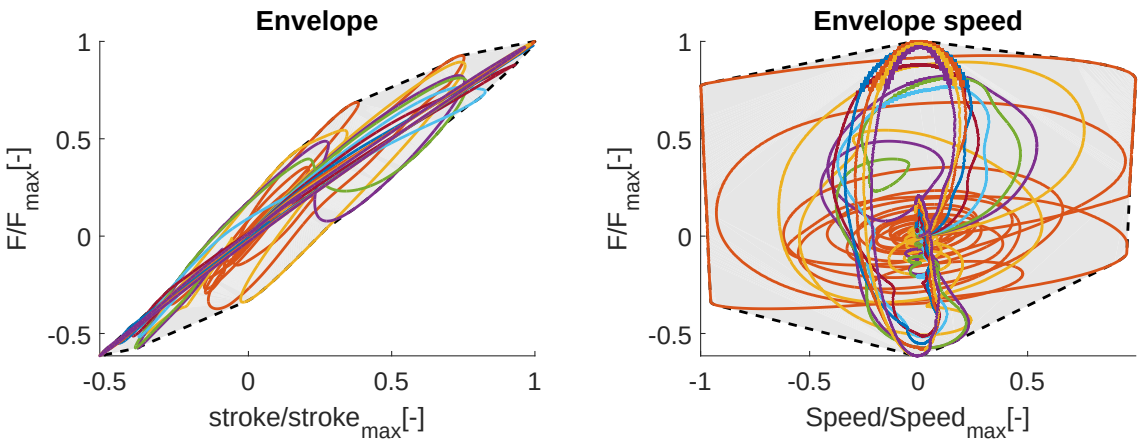


(a) Axial-stroke envelope

(b) Axial-speed envelope

Figure 17: Actuator envelopes

In order to have a redundancy on the actuation system, a double EMA system has been designed; in this way it is possible to split the required load on two actuators instead of a single one. The twin actuators guarantee a brake option in case of failure of one of them, avoiding a free surface condition.

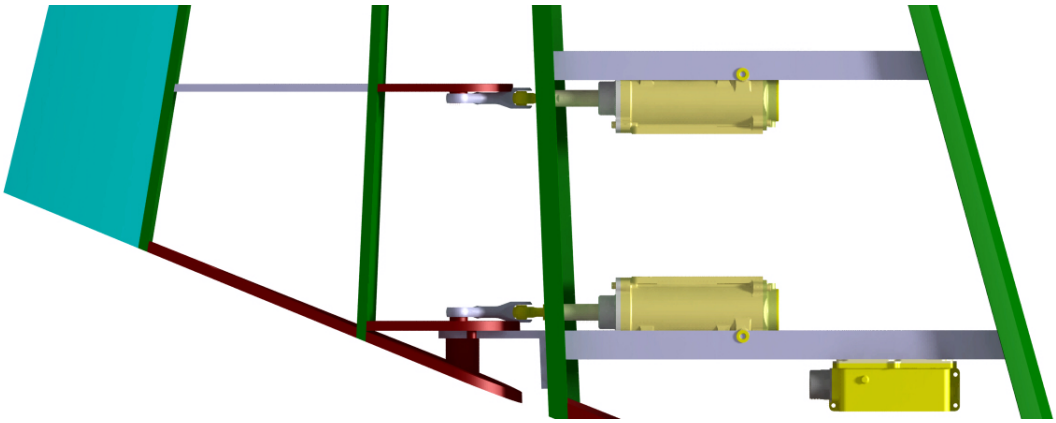

Figure 18: Double actuator configuration

## 6 CONCLUSION

The work presented shown a possible methodology for the design of a new wingtip concept, which combines the aerodynamic improvement with gust load alleviation capabilities thanks to its movable surface. The reduction of the wing root bending moment, obtained through a Static Output Feedback controller, is around 25%. This is an interesting result looking to the future, where the certification of the active controller for load control and alleviation is a relevant task; the load reduction will allow the structural engineer to design lighter structure saving mass and material. The mass-saving together with the aerodynamic performance improvement obtained, LoD ratio augmented of 0.56%, ensures a fuel saving, hence a reduction of $CO_2$ and $NO_x$ emissions.

## 7 ACKNOWLEDGMENT

The research leading to these results has received funding from the European Communitys Seventh Framework Programme (FP7/2007-2013) for the Clean Sky Joint Technology Initiative under grant agreement CSJU-GAM-GRA-2008-001 and the European Communitys Horizon 2020 - the Framework Programme for Research and Innovation (2014-2020) for the Clean Sky Joint Technology Initiative under grant agreement CS2-REG-GAM-2014-2015-01.

## 8 REFERENCES

[1] Kroo, I. (2001). Drag due to lift: concepts for prediction and reduction. *Annual Review of Fluid Mechanics*, 33(1), 587–617.

[2] Williams, D., Mann, A., and Grundy, T. (2004). Large wingtip devices-a review of activities and progress in the nexus. In *M-DAW & AWIATOR Projects 4 th European Congress on Computational Methods in Applied Sciences and Engineering (ECCOMAS), Jyvaskyla, Finland*. pp. 24–28.

[3] Mann, A. and Elsholz, I. (2005). The m-daw project-investigations in novel wing tip device design. In *43rd AIAA Aerospace Sciences Meeting and Exhibit*. p. 461.

[4] Whitcomb, R. T. (1976). A design approach and selected wind tunnel results at high subsonic speeds for wing-tip mounted winglets.

[5] Cavagna, L., Ricci, S., and Travaglini, L. (2011). Neocass: an integrated tool for structural sizing, aeroelastic analysis and mdo at conceptual design level. *Progress in Aerospace Sciences*, 47(8), 621–635.

[6] De Gaspari, A., Toffol, F., Mantegazza, P., et al. (2016). Optimal and robust design of a control surface actuation system within the glamour project. *Aerotecnica Missili & Spazio*, 95(4). doi:10.19249/ams.v95i4.288.

[7] De Gaspari, A., Mannarino, A., and Mantegazza, P. (2017). A dual loop strategy for the design of a control surface actuation system with nonlinear limitations. *Mechanical Systems and Signal Processing*, 90(2017), 334 – 349. doi:10.1016/j.ymssp.2016.12.037.

[8] Ricci, S. and al (2017). Design and wind tunnel test validation of gust load alleviation systems. In *58th AIAA/ASCE/AHS/ASC Structures, Structural Dynamics, and Materials Conference*. p. 1818.

[9] Fonte, F., Ricci, S., and Mantegazza, P. (2015). Gust load alleviation for a regional aircraft through a static output feedback. *Journal of Aircraft*, 52(5), 1559–1574.

[10] Ghasemi, S., Mosahebi, A., and Laurendeau, E. (2014). A two-dimensional/infinite swept wing navier–stokes solver. In *Proceedings of the 52nd Aerospace Sciences Meeting*. AIAA SciTech, pp. 1–11.

## COPYRIGHT STATEMENT